Eur. Phys. J. D (2021) 75:316
https://doi.org/10.1140/epjd/s10053-021-00332-z

THE EUROPEAN PHYSICAL JOURNAL D

Regular Article – Atomic and Molecular Collisions

Computing resonance energies directly: method comparison for a model potential

Jeremy U. Davis Jr. and Thomas Sommerfeld[a]

Department of Chemistry and Physics, Southeast Louisiana University, SLU 10878, Hammond, LA 70402, USA

Received 18 October 2021 / Accepted 15 December 2021 / Published online 30 December 2021

Abstract. In contrast to bound states, electronically metastable states or resonances still represent a major challenge for quantum chemistry and molecular physics. The reason lies in the embedding continuum: Bound states represent a many-body problem, while resonances represent a simultaneous scattering and many-body problem. Here we focus on so-called $\mathcal{L}^2$-methods, which treat the continuum only implicitly, but rather take the 'decaying state' perspective and emphasize electron correlation in the decaying state. These methods represent a natural extension of quantum chemistry into the metastable domain and are suitable for, say, modeling electron-induced reactions or resonant photo detachment. The three workhorse $\mathcal{L}^2$-methods are complex absorbing potentials, the stabilization method, and regularized analytic continuation. However, even for these three methods, making comparisons is less than straightforward as each method works best with a unique blend of electronic structure methods and basis sets. Here we address this issue by considering a model potential. For a model, we can establish a reliable reference resonance energy by using the complex scaling method and a discrete variable representation. Then, we can study the performance of the three workhorse methods as well as effects of more approximate Gaussian basis sets.

1 Introduction

Metastable electronic states—so-called resonances—are states unstable with respect to electron autodetachment. Resonances are characterized by their energy, the resonance position, E_r, and by their width, Γ, which represents a first-order decay constant [1–4]. In other words, a resonance posses a typical decay time $\tau = \hbar/\Gamma$—referred to as its lifetime—that is inversely proportional to its width. Resonance position and width are normally combined to their Siegert energy [5]

$$E_{res} = E_r + E_i = E_r - i\frac{\Gamma}{2}$$

which is central in many theoretical approaches. Note that the Siegert energy and the associated Siegert state represent solutions of the physical Hamiltonian with respect to purely outgoing boundary conditions, in other words, resonances are not part of the Hamiltonian's Hermitian domain.

Examples for electronic resonances include temporary anions, small dianions in the gas phase, core-ionized atoms and molecules decaying via the Auger process, the analogous Auger-like decay of inner-valence ionized clusters, doubly excited states with energies in excess of the ionization energy of the neutral, and molecules subject to field ionization [4,6–10].

It is useful to group the available computational approaches into two classes according to how the embedding continuum is treated: Class one methods solve the scattering problem explicitly, while class two methods treat the continuum only implicitly and use $\mathcal{L}^2$ wavefunctions. Examples for class one methods include the R-matrix and the complex Kohn method [11–13], examples for $\mathcal{L}^2$ methods include complex absorbing potentials (CAP) [4,14], the Hazi–Taylor stabilization (HTS) method [15–17], and the regularized analytical continuation (RAC) method [18,19].

Class one methods are the natural choice when computing cross sections; class two methods represent a more natural extension of quantum chemistry into the continuum, and with the exception of certain threshold processes [20,21], it is easier to compute potential energy surfaces or investigate electron-induced reactions. Here we will focus on class two methods: the typical workhorse methods CAP, HTS, and RAC are most frequently used in molecular physics and quantum chemistry.

However, electronic resonances represent not only a scattering, but also a many-body problem. In other words, one needs to simultaneously address the electronic continuum and electron correlation, and any

Supplementary Information The online version contains supplementary material available at https://doi.org/10.1140/epjd/s10053-021-00332-z.

[a] e-mail: thomas.sommerfeld@selu.edu (corresponding author)

computational method for electronic resonances must combine one of the continuum methods with an electronic structure method.

The combination character of any computational method for resonances has two crucial implications. First, regardless of the continuum approach, the performance of a combination method will depend drastically on how well the electronic structure method describes correlation in the bound part of the resonance and in the embedding continuum states. These state mix, and two types of balance are required: balance between calculations with different numbers of electrons (size extensive methods) and an internal balance of the calculation for the resonance [22]. For example, all continuum methods are generally more successful to describe shape resonances, while the results for Feshbach and core-excited shape resonances are mixed. Note that this is an issue of the electronic structure method and possibly the Gaussian basis set—not of the continuum method as such.

And that is not all. All three continuum methods, CAP, HTS, and RAC, are not uniquely defined, but there exist various different variants for each. Last, every electronic structure method implies a basis set, and as the different continuum methods require drastically different diffuse sets, it makes sense to distinguish the valence set from the diffuse set. Together, all these methods and variants lead to a bewildering magnitude of options.

It is then hardly surprising that *direct* method comparisons are exceedingly rare. When first introduced, any new combination is, of course, compared to the available literature, but normally two results differ in at least two aspects, say, continuum method and variant, or continuum method and electronic structure method, or continuum method and basis set. The authors are aware of only two papers that aim at a fair comparison between different continuum methods keeping the electronic structure method and basis set as similar as possible: Reference [23] compares the CAP method with analytical continuation of the coupling constant, an earlier form of the RAC method, and Ref. [24] compares the CAP method with the HTS method. At the same time, these two papers serve as a stark reminder of the large number of variants in the resonance field: References [23] and [24] use drastically different variants of the CAP methods, only remotely related electronic structure method, as well as different basis sets.

Here we address this issue by considering a model potential; in other words, the $\mathcal{L}^2$ continuum methods can be compared without choosing an electronic structure method. In addition, the model potential enables us to compute a reliable reference resonance energy by using the complex scaling (CS) method [25,26] and a discrete variable representation (DVR) [27]. Then, the three workhorse methods, CAP, HTS, and RAC as well as effects of Gaussian basis sets can be studied both independently and in conjunction.

The paper is structured as follows: In Sect. 2, we describe our model potential and briefly review the CS, CAP, HTS, and RAC methods emphasizing the common features of the four methods. Moreover, we emphasize details specific to the employed variants and discuss both the DVR and Gaussian basis sets used. The results of our comparisons are presented in Sect. 3, and Sect. 4 concludes.

2 Methods

In this section, we first discuss our model potential. Then, we describe the four continuum methods used, CS, CAP, HTS, RAC focusing on the similarities of the associated computational protocols, and the various variants of each method. Last, we describe the wavefunction representations used, DVR and Gaussian basis representations (GBRs).

2.1 Model potential

The model consists of a shifted harmonic potential times a Gaussian that forces the potential to vanish asymptotically plus an angular momentum term. In atomic units, the model reads:

$$V_M(r) = \left(ar^2 - b\right)\, e^{-cr^2} + \frac{l(l+1)}{2r^2} \tag{1}$$

where a, b, and c are parameters with $a = c = 0.028$ and $b = 1$, and we consider an angular momentum of $l = 1$. These parameters have been chosen so as to model typical molecular π^* resonances: V_M features a radial well at $r \approx 2.7$ Bohr and a 4 eV barrier at $r \approx 8.3$ Bohr, and for $l = 1$, it supports one bound state with a binding energy of -7.17 eV as well as one low-energy resonance at about 3.2 eV.

As usual, we do not solve for the radial wavefunction $R(r)$ associated with V_M directly, but transform the radial Schrödinger equation *via* the substitution $u(r) = rR(r)$. Then $u(r)$ is expanded using either a discrete variable representation (DVR) or a set of Gaussian functions leading to a GBR.

As we aim at representing the bound and the outgoing-wave part of a resonance state, we choose a simple sine DVR [28] that guarantees a uniform point density over the whole DVR grid. Specifically, we use a grid density of 15 points-per-Bohr, and the grid extends over the range $[0, r_{max}]$ where r_{max} depends on the continuum method used (large for CAP, relatively small for RAC).

The Gaussian basis sets, on the other hand, are designed to mimic typical Gaussian basis sets used in electronic structure theory. All basis functions are centered at the origin, and the number of functions is fairly small: 10 primitive valence functions with even-scaled exponents between 17 and 0.032 (even scaling factor 2) that were chosen to represent the bound ground state of V_M reasonably accurately. In the spirit of atomic-natural-orbital or correlation-consistent basis sets, the eigenfunction of the bound state is then used to contract the valence basis. In particular, we study the

uncontracted primitive set (UN) as well as a double-ζ-like (DZ) and a triple-ζ-like (TZ) set that are constructed by adding the smallest and the two smallest exponents as uncontracted functions.

For the RAC method, these valence sets are used without further augmentation; for CS, CAP, and HTS, the three basis sets are augmented with four diffuse functions, where the exponents are obtained by continuing the valence set with an even scaling factor of 1.5.

2.2 Continuum methods

We focus on four commonly used continuum methods and their mainstream variants. For the theoretical background and many more methods, the reader is referred to the book [26]. Here, we take a more practical approach and emphasize the computational protocol shared by all four $\mathcal{L}^2$ continuum methods.

To start out, the physical Hamiltonian is parametrized in one way or another:

$$\mathbf{H} \rightarrow \mathbf{H}(\lambda)$$

where λ is the parameter. Then, the actual computations consist of three major steps.

Step 1. Compute n energies for m values of λ: $E_j(\lambda_i)$, the so-called λ-trajectories of the energies.
Step 2. Identify the trajectory or trajectories associated with the resonances.
Step 3. Analyze one or two selected λ-trajectories to find E_{res}.

The major difference between the $\mathcal{L}^2$-methods involves the parametrization step 1, while the variants of each method differ mostly in the analysis step 3. The RAC method is a bit of an exception, in that many different step 1 parametrization variants exist. But despite these differences between the $\mathcal{L}^2$-methods, the overall workflow is very similar.

In an electronic structure context, step 1 takes the lion's share of the computational cost, while for a model, step 3 is often more expensive than step 1. Step 2 is often a sore spot. As a rule, identifying the 'right' trajectories requires at least some user input. While with DVR-quality data, step 2 is normally trivial and pattern recognition software will be reliable, in the context GBRs typically used in electronic structure theory, distinguishing resonances from artifacts is challenging and requires either prior knowledge or deeper analysis.

2.2.1 Complex scaling

While CAPs, the HTS method, and the RAC method are the focus of this study, CS is used to establish a reliable reference result. That is possible as—outside errors related to the basis set representation—CS is an exact theory. Complex scaling can be understood as a similarity transformation of the Hamiltonian that changes the boundary condition of Siegert states from purely outgoing wave to $\mathcal{L}^2$ so that resonance wavefunctions can be expanded in finite basis sets [25,26].

However, instead of a similarity transformation, complex scaling is most naturally written as:

$$r \rightarrow e^{i\theta} r \tag{2}$$

in other words, the variable describing the outgoing particle is multiplied by a phase. The complex-scaled Hamiltonian

$$\mathbf{H}_\theta = \mathbf{H}(e^{i\theta} r) \tag{3}$$

is no longer Hermitian, but complex-symmetric, and the continuum of the physical Hamiltonian is discretized and rotated by an angle of 2θ into the fourth quadrant of the complex energy plane [25,26]. This formulation is not only most straightforward, but also most convenient in the context of models and light atoms. In contrast, for electronic resonances of molecules, other formulations such as complex basis functions or exterior scaling are needed [26]; however, for molecules, CAPs, which can be understood as drastically approximated complex-scaling [26], remain the more popular choice.

In CS, resonances are identified as follows: As soon as rotation of the pole string uncovers the resonance energy E_{res} in the complex plane, the resonance trajectory will approach E_{res} and remain in its vicinity for a range of θ values. The details—how fast can a trajectory approach E_{res}, for which θ range does it remain close, at what θ does it depart—depend on the finite basis set used to represent $\mathbf{H}_\theta$. For a given basis set representation, the best resonance energy is obtained for:

$$\min \left| \frac{dE}{d\theta} \right| \tag{4}$$

2.2.2 Complex absorbing potentials

In the CAP method, the physical Hamiltonian is parametrized by adding a complex one-particle potential $-i\eta W$ yielding a complex-symmetric effective Hamiltonian

$$\mathbf{H}(\eta) = \mathbf{H} - i\eta W \tag{5}$$

where η is the so-called CAP strength, and the potential W must fulfill the following conditions:

$$\mathrm{Re}\{W(r)\} \geq 0 \quad \text{and} \quad \mathrm{Re}\{W(r)\} \rightarrow \infty \text{ for } r \rightarrow \infty \tag{6}$$

In general, W can be complex, in which case it must fulfill yet more conditions [14], but normally it is chosen as a real function that vanishes at the system, switches on smoothly, and then grows to infinity. A typical example is

$$W(r) = \begin{cases} 0 & : r < r_{cut} \\ (r - r_{cut})^2 & : r \geq r_{cut} \end{cases} \quad (7)$$

CAPs are best understood in the time-dependent picture: The real part of W appears as imaginary contribution to the effective Hamiltonian and therefore absorbs the outgoing particle in the region beyond r_{cut} [29,30]. In time-independent calculations, CAPs are closely related to CS: The continuous spectrum of the physical Hamiltonian is transformed into a purely discrete spectrum with $\mathcal{L}^2$ eigenfunctions [14]. In the complete basis set limit and in the limit $\eta \to 0^+$, the continuum eigenvalues are rotated on a string that depends on the functional form of W and—if uncovered by the rotation—the exact Siegert energy E_{res} of the resonance is recovered as an isolated pole.

With finite basis sets, some minimal CAP strength is needed to absorb the outgoing particle within the spatial and momentum space confinements of the basis set. Larger CAP strength should be avoided as larger η values lead to artificial reflections at the CAP boundary and by the CAP itself and therefore to a perturbation of the resonance wave function in the inner region [14,31].

The best trade-off is found by analysis of the resonance trajectories, which can be identified by its small η-velocity or the small r and W expectation values of the associated wavefunction.

In contrast to CS, one has two options: First, one can either analyze the raw trajectory or correct the raw trajectory for CAP artifacts. Second, one can analyze the complex trajectory [14,30] or consider its real and imaginary parts as real functions [32]. Hence, the CAP method has four variants, complex, uncorrected (C0), complex, first-order corrected (C1), real, uncorrected (R0), and real, first-order corrected (R1). For each of the four variants, the optimal CAP strength η_{opt} is determined by a minimum of the logarithmic speed of the considered trajectory (see refs. [14,30,32] for details).

Let us mention that the first-order correction

$$E^{(1)} = E^{(0)} + i\eta\,(W) = E^{(0)} - \eta\frac{dE}{d\eta} \quad (8)$$

can either be obtained from (W), the c-expectation value of the CAP, or from the logarithmic speed of the η-trajectory, and that it corrects for CAP artifacts in first-order perturbation theory [14,30]. Higher-order corrections have been derived but turn out to be impracticable as at the same time as CAP artifacts are explicitly corrected, basis set artifacts are implicitly enhanced [14].

2.2.3 Stabilization method

In the HTS method, the physical system is enclosed in a confining potential so that the continuum of the original Hamiltonian is discretized. The confinement can be imposed explicitly through box-boundary conditions or implicitly *via* a basis set.

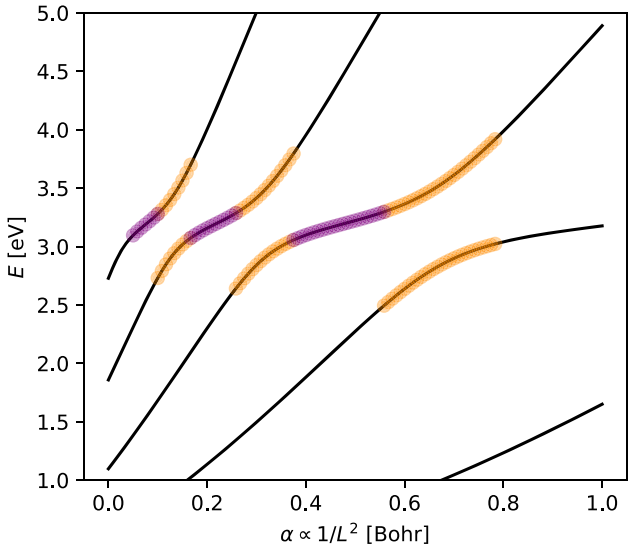

Fig. 1 Stabilization graph obtained for V_M using a DVR. The energy of all states is plotted *vs.* $\alpha = 1/L^2$, where L is the grid extent. Discretized continuum states increase approximately linearly with α, while the resonance state remains unaffected and creates a series of avoided crossings (orange) and stabilization plateaus (purple)

In the HTS method the proverbial box-size L takes the role of the parameter to be scanned in data-collection step 1, but any measure of the extent of the confinement will do. For DVR grids, the box size L is given by the grid length, and one implementation use—at fixed grid density—longer and longer grids. Alternative, one large grid can be combined with an explicit finite-depth box potential that may be smooth. However, the softer the potential and the smaller its depth, the smaller the dependency of the discretized continuum states on the box size, and the more washed out the stabilization plateaus and avoided crossings (see below).

With a GBR, the confinement and its size is less well-defined. One possible choice for a size parameter is $1/\sqrt{\alpha}$, where α is the smallest exponent in the Gaussian basis set, another is the largest eigenvalue of the position operator.

Plotting the result of the scan yields a so-called stabilization graph: $E_n(L)$ *vs.* $1/L^2$ shown in Fig. 1. The resonance reveals itself as a series of avoided crossings of a 'stable' state, whose energy is independent of $1/L^2$, with discretized continuum states, whose energy is roughly proportional to $1/L^2$ or α. Plotting $E_n(L)$ directly *vs.* L reveals the same picture, but the discretized continuum energies decrease roughly proportionally to $1/L^2$ and are strongly curved.

A first-order estimate of the resonance position can be directly obtained from the inflection points defining the centers of the plateaus. Similarly, the width can be estimated from the smallest gap of the avoided crossings corrected for the local density of states (see Refs. [33–35] and, for a thorough discussion of the history of this field, Ref. [17]).

More robust methods use stabilization graph data to establish an analytical model $E(z)$ for continuing the energy into the complex plane, where z is the complex continued variable α or L. First, an analytical model $E(z)$ is fit to the stabilization graph data $E_n(L_j)$. Then, the resonance energy E_{res} is identified from stationary points of $E(z)$:

$$\left|\frac{dE(z)}{dz}\right| = 0 \tag{9}$$

Here we investigate three models: First, general Padé approximants (GPA)

$$E^2P(z) + EQ(z) + R(z) = 0 \tag{10}$$

where P, Q, and R are polynomials in z fit to data from both branches of a crossing [16,36]. Specifically, orders of 2, 3, and 4 are used for P, Q, and R [37]. Second, a 2-by-2 model Hamiltonian $\underline{\mathrm{H}}$ is fitted to data from both branches of a crossing [38]. And third, a standard Padé approximant is fitted to data from a plateau [17,39]. In the plateau method, we increased the Padé-order systematically, and at least in the context of our model, it turned out that [4,4]-approximants represent the most robust choice as the resonance energy is practically converged and higher Padé-orders start to show occasional numerical instabilities.

Let us note that all three variants as used here assume that the resonance separates from other resonances and is sufficiently narrow to yield reasonably isolated stabilization plateaus and two-state crossings. If two resonances interact, or resonances are so broad that the crossings and plateaus affect each other, the models need to be extended by higher-order terms. To the best of our knowledge, the theoretical background has been developed for the GPA method only [16], but three-state or even higher-order models are almost never used in practice as the number of fit parameters and the number of nonphysical roots quickly increase. At least in case of broad resonances, one alternate strategy is to employ explicit box potentials. While the appeal of simplicity of exponent scaling is lost, one gains more control over the slopes of the discretized continuum states and therefore over the stabilization graph.

All three HTS variants need input data, and the results will vary somewhat with the α or L ranges chosen, in other words, with how specifically a 'crossing region' or a 'plateau region' is defined. To the best of our knowledge, the only systematic approach addressing this issue is the clustering technique introduced in Ref. [39]. Briefly, an extended data set sampling the selected plateau—or crossing—is chosen. Then, a large number of smaller data sets are created by eliminating data points at the right, the left, of both ends of the data range. For each subset, the corresponding model is fit, and stationary energies (Eq. 9) are identified. When plotted in the complex plane, these energies form a *cluster* at the predicted resonance energy, and after eliminating outliers, a statistical analysis of the cluster can be performed.

For each of the three methods, two data-selection variants were considered. A naive choice, where only a single data set based on curvature cutoffs, is used: The center of a crossing region is defined by the maximal and minimal curvatures of the two crossing curves, while the center of a plateau is defined by the vanishing curvature of the single stable curve. The two regions are separated at the average curvature points, that is, where the extreme curvatures drop to half their values (c.f. Fig. 1).

A multi-data-set clustering variant that uses the 30% and 70% curvature extrema drop-off points results in extended ranges and overlapping crossing and plateau regions: Starting from these extended data ranges a clustering analysis similar to Ref. [39] is performed; however, we always keep the center of the structure, that is, while data points are systematically eliminated from the right and left of the data range, the central point is always kept.

Complex stationary points (see Eq. 9) can be identified by various means. For the 2-by-2 model Hamiltonian, these points can be found analytically [38], while for the GPA and plateau methods numerical methods are required (see, e.g. [16,17]). Here we employ Newton's method, and in the interest of replicability, let us mention a few details of our computational protocol.

- To enhance numerical stability, as a first step, the actual α or z-range is rescaled to $[0, 1]$ (c.f. Fig. 1).
- Newton searches are started on a 10-by-10 search grid loosely defined by the z-range of the investigated plateau or crossing region as defined above. In practice, we double the naive z-range on the real axis and search a square area starting on the real axis and extending down into the fourth quadrant.
- Newton searches converging in 10 steps or less to points in the fourth quadrant are accepted, and a list of unique stationary points is established.
- Applying this algorithm to our model typically yields a single stationary point for the standard [4,4] Padé approximants of the plateau method, and two or three stationary points for [2,3,4]-GPAs. For the naive variant, these two or three GPA energies are averaged [37].
- For the clustering variants, all stationary energies associated with all data subsets are kept. For the model potential, the cluster is easily identified by averaging, and typically only one discard-outliers, recompute-the-average iteration is needed [39].

2.2.4 Regularized analytical continuation

In the RAC method, an artificial attractive potential U is added to the physical Hamiltonian

$$\mathbf{H}_\lambda = \mathbf{H} + \lambda U \tag{11}$$

where λ is the strength parameter varied in data-collection step 1 (see refs. [18,40,41] as well as chapter 5 of Ref. [42]). However, it is also possible to scale the attractive part of the physical potential.

In principle, U must be a short-range potential [1]; in particular, Coulomb potentials disrupt the connection between resonances and bound states [43]. Nonetheless, in practical electronic structure calculations, scaling the nuclear charges has turned out to work well [18,40,41,44,45] presumably because representation of the Coulomb potential in the compact Gaussian basis sets suppresses the long-range part of the interaction. In fact, in a Gaussian basis set, attractive Coulomb potentials and explicitly attenuated Coulomb potentials behave effectively identically [46,47].

Here, we use three different stabilizing potentials:

1. Instead of adding an explicit potential U_1, the attractive part of of V_M (Eq. 1) is increased: $b \to (1+\lambda)b$ (b-scaling). As part of the physical potential itself is scaled, this approach is loosely analogous with scaling nuclear charges in electronic structure theory.
2. As motivated by electronic structure calculations, an attractive Coulomb potential, $U_2 = -1/r$, is added to $\mathbf{H}$.
3. A finite-depth confining potential $U_3 = \exp(-(2d)^2/r^2) - 1$ (soft-box) is added to $\mathbf{H}$, a choice new in the RAC context. U_3 forms an amazingly flat region of depth -1 localized at the origin. Its soft wall starts to climb at about d, and the half depth is reached at about $2.4d$. For V_M, we use $d = 3$ Bohr.

For each U_k, λ is then increased until the resonance crosses the threshold and becomes a bound state and then further increased until the resulting bound state exhibits an energy of at least $-7E_r$. Clearly, this step requires either prior knowledge of the resonance position, say, from a calculation with a smaller basis set or a larger step size in λ. However, this concern is valid only in the electronic structure context where step 1—collecting data—is costly. Here, all steps are computational inexpensive, and iterating the procedure once is unproblematic.

In RAC calculations, step 2—identifying the resonance trajectory—tends to be simple as the resonance state is normally associated with the most compact wavefunction and therefore with the λ-trajectory that shows the largest downward slope. In practical RAC calculations, compact basis sets are used and only the ground state is computed, which gives RAC special status among the continuum methods. On the one hand, RAC is designed to work only for resonances with non-vanishing angular momentum and only for 'low-energy' resonances as the threshold behavior at the crossing from bound to unbound state is analytically continued [42]. On the other hand, RAC needs only ground state input data enabling combinations with a much wider variety of electronic structure method than CAP or HTS.

In step 3, the bound energies are fit to an inverse Padé approximant tailor-made for describing the threshold behavior of resonances in the complex momentum plane [18,19]. The most widely used approach is the [3,1]-Padé approximant [18,44,45,48]

$$\lambda(\kappa) = \lambda_0 \frac{\left(\kappa^2 + 2\alpha^2\kappa + \alpha^4 + \beta^2\right)\left(1 + \delta^2\kappa\right)}{\alpha^4 + \beta^2 + \kappa\left(2\alpha^2 + \delta^2\left(\alpha^4 + \beta^2\right)\right)} \quad (12)$$

Here, $\kappa^2 = -E$ (bound energies are negative), α, β, δ, and λ_0 are positive fit parameters, and λ is the strength parameter from Eq. (11). Note that, instead of $\kappa(\lambda)$, the inverse function $\lambda(\kappa)$ is fit.

Higher-order approximations exist; however, only certain orders fulfill the correct threshold conditions [19], and for higher orders, the nonlinear fits become quickly numerical unstable [44]. We note that [3,2]-Padé approximants have been recommended for singular stabilization potentials such as Coulomb [19]. The [3,2]-Padé ansatz is almost identical to Eq. (12); however, the denominator is extended with an $\epsilon^2\kappa^2$ term where ϵ is a fifth parameter. For the Coulomb potential U_2, we show both RAC[3,1] and RAC[3,2] results.

Regardless of the Padé-order used, after the parameters have been fit to the data, the resonance energy is directly obtained from α and β:

$$E_r = \beta^2 - \alpha^4 \qquad \Gamma = 4\alpha^2\beta \quad (13)$$

Similar to the HTS variants, RAC results depend on the input data range. To minimize the influence of any avoided crossings close to threshold, relatively compact DVR and GBR representations are used and input energies bound by less than -0.5 eV are discarded. (See the analysis of Fig. 2 in Ref. [18].) Moreover, we perform the following averaging procedure.

- A fairly precise estimate, $E_r^{(0)}$, is obtained by fitting to all available energies below -0.5 eV.
- The fitting procedure is repeated for all data ranges from $[-0.5, -4E_r^{(0)}]$ to $[-0.5, -7E_r^{(0)}]$, and the results are averaged using the quality of the respective fit, χ^2, as weights. For DVR and UN, the standard deviations of this procedure are quite small (less than $\pm 1\%$ for E_r, a bit larger for Γ). For TZ and DZ, the standard deviations of E_r are still acceptable ($\pm 2\%$); however, as the width is much smaller than the position, the relative deviation of E_i becomes significant ($\pm 30\%$) for these basis sets.

3 Results

In this section, we investigate the 3.2 eV resonance of the model potential with the three workhorse continuum methods CAP, HTS, and RAC. Moreover, we study the progression DVR, uncontracted GBR, GBRs of triple and double-ζ quality. We start with establish-

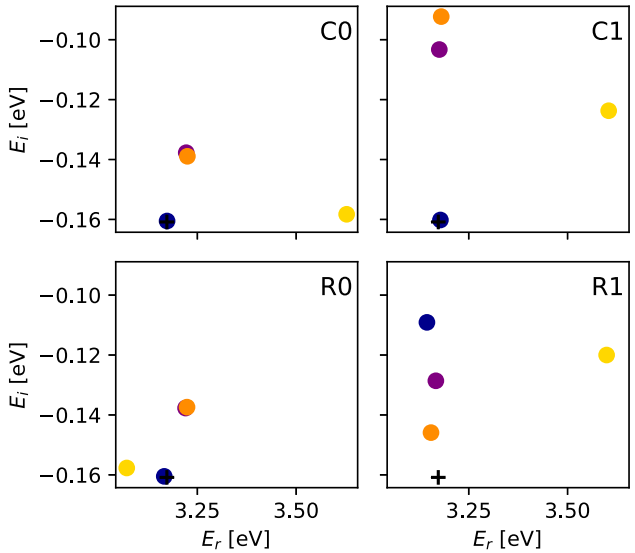

Fig. 2 CAP resonance energies of V_M. Each panel shows results obtained with the indicated analysis method, and the colors code the basis set: DVR, in blue; UN, TZ, and DZ in purple, orange, and yellow. The CS reference energy is indicated by a black cross

Table 1 Complex scaling results for the model potential V_M. Energies in eV and angles in degrees

	E_r	$\Gamma/2$	θ_{opt}	$\left\vert\frac{dE}{d\theta}\right\vert$
DVR[a]	3.172963	−0.1608477	41	$1.4\,10^{-6}$
DVR[b]	3.172956	−0.1608490	34	$1.4\,10^{-6}$
DVR[c]	3.172944	−0.1608467	26	$1.4\,10^{-6}$
UC	3.169	−0.144	11.0	0.0049
TZ	3.099	−0.068	4.6	0.0026
DZ	3.102	−0.051	2.2	0.024

[a] Grid length 25 Bohr.
[b] Grid length 30 Bohr.
[c] Grid length 35 Bohr

ing a reference value with CS/DVR and briefly consider basis-set effects in the context of CS.

The CS/DVR combination is expected to yield highly reliable resonance energies, and the results for the model potential in Table 1 demonstrate that the resonance trajectory essentially slows to a halt as the derivative of the energy with respect to the rotation angle becomes insignificant. Moreover, grid extent impacts only the optimal rotation angle, but has virtually no effect on the resonance energy. Accordingly, the CS reference resonance energy can be stated with six significant digits: $E_{res} = 3.17295\,\text{eV} - 0.160847i\,\text{eV}$, where the observed variation in the last digits is in the order of 2.

In addition to providing a reference value, CS can be used as testing ground for GBR (Table 1). For all Gaussian basis sets, the magnitude of the derivative $\frac{dE}{d\theta}$ at θ_{opt} is substantially larger than for DVR: at best three orders of magnitude, for the DZ set even four orders of magnitude. Correspondingly, the resonance energies are less well converged, and only the UC resonance energy is close to the DVR reference value. This is expected: Straightforward CS—as opposed to exterior scaling—requires a flexible basis set at all distances, and contracted GBR are simply unsuitable for straightforward CS.

3.1 Complex absorbing potentials

Results for the model potential in Eq. (1) obtained with a CAP combined with DVR or GBR and analyzed with the four different variants are displayed in Fig. 2. The data allow us to analyze a number of different trends.

1. Combined with a DVR, a CAP performs exceedingly well. In particular, the C0 energy is on top of the CS reference marker; however, both C1 and R0 are tight runners up, and one has to pay close attention to see that the CS marker is not quite dead center on the respective CAP/DVR points. The only odd one out is the R1 analysis: The predicted width is too small.
2. Similar to CS, GBR results are generally less accurate than DVR resonance energies. Still, CAP/GBR widths are significantly more reliable than their CS/GBR counterparts, and while CAPs are by no means perfect, they seems far more robust to basis set deficiencies than CS.
3. The small differences between the UN and TZ results show that CAPs work well without extra flexibility in the valence region. However, the off-target DZ results show that some flexibility in the outer valence region is needed.
4. In particular, the C0/C1 difference shows that correcting for CAP artifacts does not necessarily improve the resonance energy. In fact, regardless of basis set, C0 is superior to C1 if only slightly so (for DVR).
5. While C0, C1, and for the most part R0 behave in predictable systematic manner, R1 does not follow this trend. Currently, we have not got any explanation for this behavior.

The data in Fig. 2 have been obtained with fixed cutoff radii of the CAP, $r_{cut} = 15$ Bohr for DVR and $r_{cut} = 7$ Bohr for GBR. While for both DVR and GBR the r_{cut}-dependence of the resonance energy has been investigated previously [31,49–51] trends have neither been compared across different analysis schemes, nor have GBR results been compared to reliable reference data. Of course, this question is most relevant for GBRs; unless DVR grids are chosen too short or with too low grid density, the exact position is rather unimportant. (The optimal position depends on the kinetic energy of the outgoing particle anyway.) In contrast, molecule-centered GBRs are at best able to describe a few oscillations of an outgoing wave, and the placement of the CAP is critical.

The resonance energy obtained with different cutoff radii and all four CAP analysis schemes are indicated

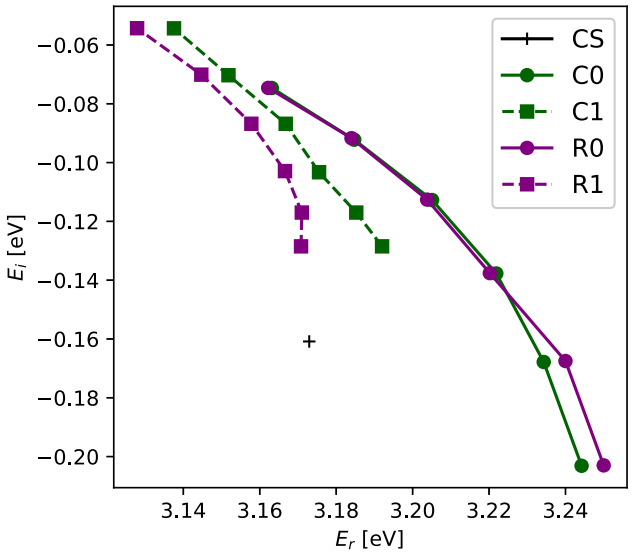

Fig. 3 CAP resonance energies of V_M computed with the UN Gaussian basis set and different CAP cutoff radii $r_{cut} = 5-10$ Bohr in steps of 1 Bohr. For all analysis methods, the smallest cutoff radius, $r_{cut} = 5$ Bohr, is associated with the most negative E_i or largest width. Reducing r_{cut} reduces the predicted width as well as the difference between the zeroth and first-order predictions for E_{res}. The CS reference result is indicated by a black cross

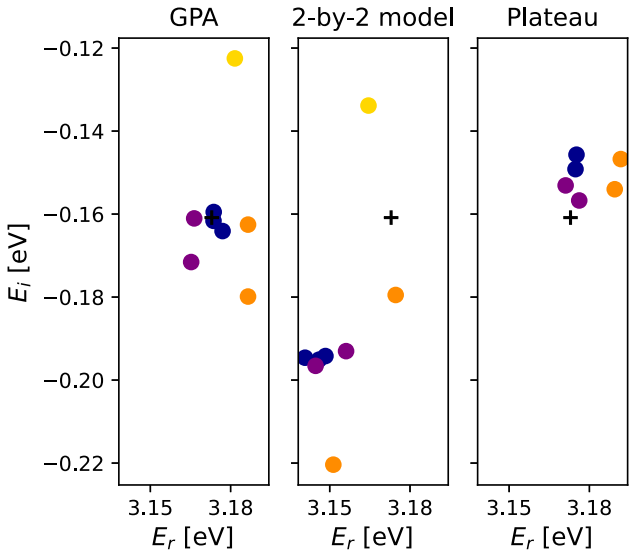

Fig. 4 HTS resonance energies of V_M. Each panel collects results from the analysis method indicated, and a clustering analysis was used for all methods. The colors code the basis set: DVR, in blue; UN, TZ, and DZ in purple, orange, and yellow. The CS reference energy is indicated by a black cross

as r_{cut}-trajectories in Fig. 3. Smaller r_{cut} values imply stronger interactions with the CAP and correspond for each r_{cut}-trajectory to the most negative imaginary parts. The smallest cutoff radius is $r_{cut} = 5$ Bohr is 'dangerously' small as the CAP penetrates well into the inner region—the classical turning point at E_r is essentially 7 Bohr—and the analysis schemes start to show numerical instabilities. Moreover, small r_{cut} values lead to large first-order corrections indicating increasingly unreliable CAP results.

Larger r_{cut} values in the order of 10 Bohr, on the other hand, are associated with numerically stable analysis schemes and small first-order corrections. These advantages, however, are deceptive, as the predicted widths are far too small, most likely owing to the inability of the GBR to describe the oscillations of an outgoing wave into the CAP region: At the very minimum, one full oscillation in the CAP region is needed to absorb an outgoing wave, and for practical CAPs the number is larger [14,31]. The 3.2 eV resonances show a wavelength of roughly 2 Bohr. GBRs modeling realistic electronic structure sets are obviously incapable of describing multiple oscillations to reach the CAP and then additional oscillations in the CAP region itself.

While this is a clear shortcoming of the GBR—not of the CAP method as such—there seems to be unfortunately no obvious method to locate a good trade-off between a CAP that penetrates too far into the interior region and a CAP that is located too far out for the GBR at hand. Indeed, it seems as if the 'best' results are obtained with r_{cut} values that balance the analysis methods at the brink of numerical instability, but that hardly translates into a well-defined criterion. In electronic structure calculations, r_{cut} is normally chosen in the order of typical van der Waals radii or even explicitly set to the radial extent of the parent wavefunction [51,52].

3.2 Stabilization method

Results from analyzing stabilization graph (c.f. Fig. 1) for our model potential are collected in Fig. 4 and in the supplementary material, Fig. S1.

We begin with the DVR results. The DVR stabilization plot (Fig. 1) shows two complete plateaus and three complete crossings. Accordingly, the GPA and 2-by-2 model Hamiltonian panels of Fig. 4 show three DVR points, while the plateau panel shows only two. For the GPA method, these three data points cluster very closely around the CS reference value demonstrating the flexibility of a [2,3,4]-GPA in performing the analytical continuation. In contrast, fitting a 2-by-2 model Hamiltonian to the same data set yields only satisfactory agreement: At least for V_M, the 2-by-2 model Hamiltonian predicts too small resonance positions and too large widths. Last, the plateau method predicts excellent resonance positions, but somewhat too small widths.

Turning to GBRs, as expected, the performance of all three analysis methods tends to decline. Yet, this trend is anything but uniform. As the DZ set turns out to introduce too many artifacts, let's focus initially on the UN and TZ sets. For the GPA/UN and GPA/TZ combinations, one of the available crossings yields acceptable results, while the width from the other crossing is somewhat too large. This trend is much

more pronounced for naive data selection (see supplementary material, Fig. S1), and at least for our stabilization plots, the 'better' crossing is associated with the higher curvatures and accordingly the smaller α or larger L values. For the 2-by-2 model Hamiltonian, both UN crossings yield results close to the DVR results, while both TZ crossings show substantial differences. Thus, it seems that the 2-by-2 model Hamiltonian is more sensitive to the overall basis set quality than to the crossing itself. Last, for the plateau method, all UN and TZ results cluster closely around the DVR results.

In contrast to the UN and TZ sets, the DZ set seems to be too inflexible to yield a stabilization plot of sufficient quality. While one of the crossings still predicts results within the ranges of Fig. 4, other DZ results are wildly scattered with real parts as high as 4 eV and imaginary parts as low as 0.05 eV. To represent the resonance and the discretized continuum in a quantitative manner, a GBR clearly needs more than DZ flexibility in the 'outer valence region'.

Last, let us comment on three more technical aspects of the stabilization method, the results of a naive data set selection and the clustering analysis. Figure S1 in the supplementary material compares the naive and the clustering variants. The following trends can be observed:

- DVR resonances are almost unaffected. In other words, for good basis sets, the curvature-determined range defines a plateau or crossing region well.
- For GBRs the impact of a clustering analysis is method dependent. GPA resonances energies are significantly improved for low-curvature crossings and TZ basis sets. No large effect is seen for the 2-by-2 model Hamiltonian. Plateau resonance energies are significantly improved. In other words, for both the GPA and the plateau method a clustering analysis is well-worth undertaking.

The second comment pertains to the 'clusters' of stationary energies produced by the different input data subsets. Plots can be found in the supplementary material, Figs. S2, S3, S4, and S5, and we analyze these clusters using two color codings. In all four figures, the energies in the left panel are color coded according to the number of eliminated points when creating input sets, where dark colors indicate larger and light colors indicate smaller subsets. Higher data to parameter ratios—more over-defined fits—are expected to lead to higher-quality fits as noise and over-fitting are less of an issue, and the dark points show indeed a smaller scatter, in particular, for the plateau method.

The stationary energies in the left panel are color coded. Dark colors indicate that the number of points eliminated from the right and the left is equal or similar; light color indicates very unsymmetrical eliminations. Again, there is a clear trend: Symmetrical sets scatter less than unsymmetrical ones.

We are aware that this is just one example and a model potential at that, however, provided these trends turn out to be more general, an improved protocol may either select only sufficiently over-defined reasonably symmetric data sets or introduce a weighted averaging procedure that emphasizes over-defined and symmetric data sets.

The last comment about the clustering method pertains specifically to the GPA method. Figures S2 and S5 in the supplementary material show that the results presented in Fig. 4 do not reflect a typical stationary energy. Quite the opposite, each individual stationary energy is quite far from the CS reference energy (see Figure S2). However, normally each selected data set contributes two stationary energies, which—as the naive variant shows—average to an energy close to the reference result. In other words, each input data subset produces a pair of stationary states that connect across the correct result.

3.3 Regularized analytic continuation

For the RAC method, the focus shifts from the analysis step 3 to the data-collection step 1. The analysis is straightforward (Sect. 2.2.4), the only quirk being the RAC[3,1] *vs* RAC[3,2] comparison for the Coulomb stabilization. The main comparison, on the other hand, involves different stabilizing potentials U_k used in step 1.

The RAC resonance energies for b-scaling, Coulomb, and soft-box stabilizing potentials U_k are displayed in Fig. 5. Since the scales are different in every panel, discussing Fig. 5 is less straightforward than for the corresponding CAP or HTS figures (Figs. 2 and 4).

We start with b-scaling. The DVR and UN results cluster at approximately $3.3 - 0.33\mathrm{i}$ eV, in other words, b-scaling predicts about 5% too high positions and 50% too high widths. Combining a TZ with b-scaling yields unacceptably large errors in the position, and DZ basis sets predict vanishing width.

For the Coulomb potential, the quality depends critically on the Padé approximation; however, none of the Coulomb results are convincingly close to the reference value (see the scales in the second panel of Fig. 5). RAC[3,1] combined with DVR or UN predicts far too small positions (below 3 eV) and far too large half widths (above 0.5 eV). For TZ or DZ, RAC[3,1] predicts vanishing width. As recommended in Ref. [19], RAC[3,2] performs significantly better. For DVR and UN, the resonance position is acceptable, yet the widths are either significantly too large or too small. Realistic basis sets of TZ or DZ quality yield results with unacceptably large errors or even vanishing widths. Let us note that the dramatic difference between RAC[3,1] and RAC[3,2] is likely context dependent. For example, Ref. [18] as well as our own experience suggests only minor differences between RAC[3,1] and RAC[3,2] in typical electronic structure calculations.

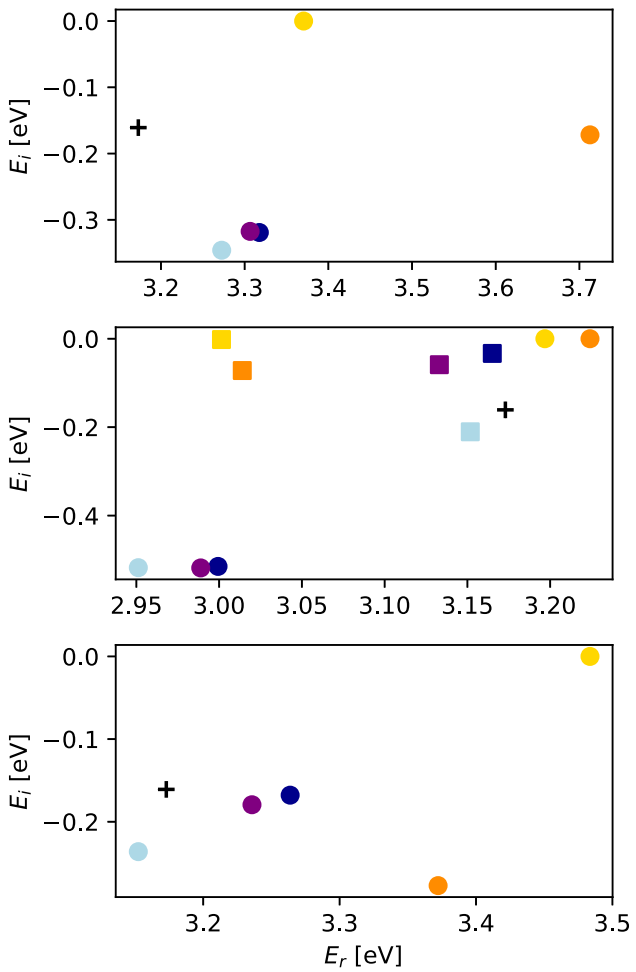

Fig. 5 RAC resonance energies of V_M. From the top, the panels collect results for each stabilizing potential: U_1, b-scaling; U_2, Coulomb; U_3, soft-box. The circles represent RAC[3,1] results; for the Coulomb potential RAC[3,2] is also shown (squares). Color codes refer to different basis set representations: DVR, $r_{max} = 12$ and 20 Bohr in dark and light blue; UN, TZ, and DZ in purple, orange, and yellow. The CS reference energy is indicated by a black cross. Note the different scales of each panel

The last panel of Fig. 5 collects the soft-box results. Again, the DVR and UN resonance energies 'cluster,' yet this time the imaginary parts of the more compact representations are very close to the reference result. In contrast, the predicted real parts are significantly too high. Again, the RAC/TZ resonance energy is far off target, and RAC/DZ predicts a zero width.

In summary, out of the three stabilizing potentials investigated, two combinations predict acceptable resonance energies: RAC[3,2] with a Coulomb stabilization, and RAC[3,1] with a soft-box stabilization. Moreover, both combinations perform satisfactorily only if DVRs or high-quality GBRs are employed. RAC results from TZ basis sets are qualitatively correct, but less useful for quantitative purposes.

4 Summary and conclusions

Using a spherical model potential, the three workhorse $\mathcal{L}^2$-methods for resonance states have been compared in detail. In contrast to electronic structure theory, for the model potential, a reliable reference value is readily available, and the three methods with their multiple variants can be compared using near perfect as well as less than perfect $\mathcal{L}^2$-basis sets: DVRs and GBRs.

Of course, strictly speaking all conclusions are valid only in the context of our model potential, and it is presently unclear to what extent generalizations to electronic structure theory or other contexts are possible. However, the authors do have considerable experience with CAP, HTS, and RAC calculations in quantum chemistry, and at least by-eye, the GBR η-trajectories, stabilization plots, and λ-trajectories observed for the model look deceptively similar to their electronic structure analogous.

Within a certain spatial range, DVRs provide a highly accurate description of the resonance and its embedding discretized continuum, and basis set errors can be neglected in comparison with other approximations. If such a representation is used, three CAP variants as well as the GPA variant of the HTS method predict resonance energies in close agreement with the CS reference value, and the plateau variant of the HTS method is a very a close runner up. The forth CAP variant as well as the 2-by-2 model Hamiltonian analysis of the HTS shows satisfactory agreement—for both the relative deviation of the imaginary part is larger than 20%.

In contrast, RAC resonance energies agree only qualitatively with the CS reference value. To be fair, for the RAC method, instead of comparing analysis variants, we varied the stabilization potentials used in the data accumulation step. It may well be that other stabilizing potentials will give better agreement with the CS resonance energy. Moreover, contrary to the trend observed for electronic structure and GBRs [18], RAC resonance energies for the model potential depend strongly on the extent of the DVR grid. We conclude that at least for this example the RAC method is sensitive to the specific conditions: the combination of the grid extent and the stabilizing potential.

Turning to GBRs, the performance of all methods and all variants must deteriorate as the used GBRs were specifically designed to mimic typical basis sets in electronic structure theory. Thus, GBRs lead to far more compact representations (in the sense of matrix dimensions) but also to a low-quality discretized continuum (representable number of oscillations of an outgoing waves). The key message here is that some method variants fare considerably better than others: They are more robust with respect to basis set deficiencies.

The best performance in this respect is shown by the plateau variant of the HTS method. Close competitors are the two uncorrected CAP variants as well as the GPA variant, but only for certain crossings. Two trends are worth noting: First, correcting CAP calculations for

CAP artifacts as frequently done in electronic structure theory might not always be a good idea. At least for the present model potential, the trade-off between correcting for the CAP artifacts at the cost of enhancing the basis set error (c.f. [14]) is not worth it. Second, augmented DZ basis sets yield at best qualitatively correct resonance energies. This conclusion is method and variant independent—the single outer-valence function of a DZ sets seems to be too inflexible to properly connect the valance and the diffuse sets to a quantitatively useful discretized continuum basis.

Let us briefly comment on generalizing our findings to electronic structure theory, where a 'method' has three ingredients: an $\mathcal{L}^2$ continuum method, an electronic structure method, and a basis set. From our model potential, it is immediately obvious that simply stating an $\mathcal{L}^2$-method is insufficient; at the very least, the variant must be specified. But to guarantee that other researchers can replicate a calculations, it is even necessary to specify the exact computational protocol in the $\mathcal{L}^2$-method data-analysis step. The simple reason behind this need is that $\mathcal{L}^2$-methods lack the standardization of electronic structure methods and basis sets. Computational studies of resonances are replicable if all three ingredients are well defined.

Acknowledgements Support from the National Science Foundation under Grant No. 1856775 is gratefully acknowledged.

Author contributions

All authors contributed equally to the paper.

Data Availability Statement "This manuscript has data included as electronic supplementary material".

References

1. V.I. Kukulin, V.M. Krasnopolsky, J. Horáček, *Theory of resonances* (Kluwer Acedmic Publishers, Dordrecht, The Netherlands, 1989), pp. 88–133
2. K.D. Jordan, V.K. Voora, J. Simons, Negative electron affinities from conventional electronic structure methods. Theor. Chem. Acc. **133**, 1445–1 (2014)
3. J.M. Herbert, The quantum chemistry of loosely-bound electrons, in Reviews in Computational Chemistry, Vol. 28, edited by A. L. Parrill and K. B. Lipkowitz (Wiley, Hoboken, NJ, USA, 2015) pp. 391–517
4. T.-C. Jagau, K.B. Bravaya, A.I. Krylov, Extending quantum chemistry of bound states to electronic resonances. Annu. Rev. Phys. Chem. **68**, 525 (2017)
5. A.J.F. Siegert, Phys. Rev. **56**, 750 (1939)
6. J.D. Gorfinkiel, S. Ptasinska, Electron scattering from molecules and molecular aggregates of biological relevance. J. Phys. B **50**, 182001–1 (2017)
7. J.U. Davis Jr., Q.M. Phung, T. Yanai, M. Ehara, T. Sommerfeld, Lifetimes of be_3^{2-} and mg_3^{2-} cluster dianions. J. Phys. Chem. A **125**, 3579–3588 (2021)
8. P. Kolorenč, V. Averbukh, Fano-adc(2,2) method for electronic decay rates. J. Chem. Phys. **152**, 214107 (2020)
9. A. Ghosh, N. Vaval, Geometry-dependent lifetime of interatomic coulombic decay using equation-of-motion coupled cluster method. J. Chem. Phys. **141**, 234108–1 (2014)
10. P. Hoerner, W. Li, H.B. Schlegel, Angular dependence of strong field ionization of 2-phenylethyl-n, n-dimethylamine (penna) using time-dependent configuration interaction with an absorbing potential. J. Phys. Chem. A **124**, 4777 (2020)
11. C.W. McCurdy, T.N. Rescigno, B.I. Schneider, Interrelation between variational principles for scattering amplitudes and generalized R-matrix method. Phys. Rev. A **36**, 2061 (1987)
12. C. Winstead, V. McKoy, A.A. Noyes, Electron scattering by small molecules. Adv. Chem. Phys. **96**, 103 (1996)
13. P.G. Burke, In Many-body Atomic Physics, edited by M. Baer and G. D. Billing (Cambridge University Press, NewYork, 1998) pp. 376–401, pp. 305–324
14. U.V. Riss, H.-D. Meyer, Calculation of resonance energies and widths using the complex absorbing potential method. J. Phys. B **26**, 4503 (1993)
15. A.U. Hazi, H.S. Taylor, Stabilization method of calculating resonance energies: Model problem. Phys. Rev. A **1**, 1109 (1970)
16. J.S.-Y. Chao, M.F. Falcetta, K.D. Jordan, Application of the stabilization method to the $N_2^-(1^2\Pi_g)$ and $Mg^-(1^2P)$ temporary anion states. J. Chem. Phys. **93**, 1125 (1990)
17. A. Landau, I. Haritan, P.R. Kaprálová-Ždánská, N. Moiseyev, Atomic and molecular complex resonances from real eigenvalues using standard (hermitian) electronic structure calculations. J. Phys. Chem. A **120**, 3098 (2016)
18. J. Horáček, I. Paidarová, R. Čurík, On a simple way to calculate electronic resonances for polyatomic molecules. J. Chem. Phys. **143**, 184102–1 (2015)
19. T. Bárta, J. Horáček, Calculation of resonances by analytical continuation: role of asymptotic behavior of coupling function. Phys. Scr. **95**, 065401 (2020)
20. W. Domcke, Theory of resonance and threshold effects in electron-molecule collisions: The projection-operator approach. Phys. Rep. **208**, 97 (1991)
21. H. Morgner, The validity of the local approximation in Penning ionisation as studied by model calculations. Chem. Phys. **145**, 239 (1990)
22. Q.M. Phung, Y. Komori, T. Yanai, T. Sommerfeld, M. Ehara, Combination of a voronoi-type complex absorbing potential with the xms-caspt2 method and pilot applications. J. Chem. Theory Comput. **16**, 2606 (2020)
23. T. Sommerfeld, M. Ehara, Short-range stabilizing potential for computing energies and lifetimes of temporary anions with extrapolation methods. J. Chem. Phys. **142**, 034105 (2015)
24. M. Thodika, M. Fennimore, T.N.V. Karsili, S. Matsika, Comparative study of methodologies for calculating

metastable states of small to medium-sized molecules. J. Chem. Phys. **151**, 244104 (2019)
25. W.P. Reinhardt, Complex coordinates in the theory of atomic and molecular structure and dynamics. Ann. Rev. Phys. Chem. **33**, 223 (1982)
26. N. Moiseyev, *Non-hermitian quantum mechanics* (Cambridge University Press, Cambridge, UK, 2011)
27. J.C. Light, Discrete variable representation in quantum dynamics. In Time–Dependent Quantum Molecular Dynamics, edited by J. Broeckhove and L. Lathouwers (Plenum Press, New York, 1992) pp. 185–199
28. D.T. Colbert, W.H. Miller, J. Chem. Phys. **96**, 1982 (1992)
29. G. Jolicard, E.J. Austin, Optical potential stabilisation method for predicting resonance levels. Chem. Phys. Lett. **121**, 106 (1985)
30. R. Santra, L.S. Cederbaum, Non-Hermitian electronic theory and application to clusters. Phys. Rep. **368**, 1 (2002)
31. U.V. Riss, H.-D. Meyer, Investigation on the reflection and transmission properties of complex absorbing potentials. J. Chem. Phys. **105**, 1409 (1996)
32. T.-C. Jagau, D. Zuev, K.B. Bravaya, E. Epifanovsky, A.I. Krylov, A fresh look a resonances and complex absorbing potentials: density matrix-based approach. J. Phys. Chem. Lett. **5**, 310 (2014)
33. C.H. Maier, L.S. Cederbaum, W. Domcke, A spherical-box approach to resonances. J. Phys. B **70**, L119 (1980)
34. J. Simons, J. Chem. Phys. **75**, 2465 (1981)
35. P.-O. Löwdin, Approximate calculation of lifetimes of resonance states in the continuum from real stabilisation graphs. Int. J. Quant. Chem. **27**, 495 (1985)
36. M.F. Falcetta, L.A. DiFalco, D.S. Ackerman, J.C. Barlow, K.D. Jordan, Assessment of various electronic structure methods for characterizing temporary anion states: Application to the ground state anions of n_2, c_2h_2, c_2h_4, and c_6h_6. J. Phys. Chem. A **118**, 7489 (2014)
37. K.D. Jordan, Private communications (2021)
38. B.J. Carlson, M.F. Falcetta, S.R. Slimak, K.D. Jordan, A fresh look at the role of the coupling of a discrete state with a pseudocontinuum state in the stabilization method for characterizing metastable states. J. Chem. Phys. Lett. **12**, 1202 (2021)
39. A. Landau, I. Haritan, The clusterization technique: A systematic search for the resonance energies obtained via padé. J. Phys. Chem. A **123**, 5091 (2019)
40. J. Horáček, P. Mach, J. Urban, Calculation of s-matrix poles by means of accc: 2-pi-g of n2-. Phys. Rev. A **82**, 032713 (2010)
41. J. Horáček, I. Paidarová, R. Čurík, Determination of the resonance energy and width of the $^2b_{2g}$ shape resonance of ethylene with the method of analytic continuation of the coupling constant. J. Phys. Chem. A **118**, 6536 (2014)
42. V.I. Kukulin, V.M. Krasnopolsky, J. Horáček, *Theory of resonances* (Kluwer Acedmic Publishers, Dordrecht, The Netherlands, 1989)
43. W. Domcke, Analytic theory of resonances and bound states near coulomb thresholds. J. Phys. B **16**, 359 (1983)
44. R. Čurík, I. Paidarová, J. Horáček, The $2\pi g$ shape resonance of acetylene anion: an investigation with the rac method. Eur. Phys. J. D **70**, 146 (2016)
45. P. Nag, R. Čurík, M. Tarana, M. Polášek, M. Ehara, T. Sommerfeld, J. Fedor, Resonance states in cyanogen nccn. Phys. Chem. Chem. Phys. **22**, 23141 (2020)
46. A.F. White, M. Head-Gordon, C.W. McCurdy, Stabilizing potentials in bound state analytic continuation methods for electronic resonances in polyatomic molecules. J. Chem. Phys. **146**, 044112 (2017)
47. T. Sommerfeld, J.B. Melugin, P. Hamal, M. Ehara, Resonance energies and lifetimes from the analytic continuation of the coupling constant method: Robust algorithms and a critical analysis. J. Chem. Theory Comput. **13**, 2550 (2017)
48. R. Čurík, I. Paidarová, J. Horáček, Shape resonances of be^- and mg^- investigated with the method of analytic continuation. Phys. Rev. A **97**, 052704 (2018)
49. T. Sommerfeld, U.V. Riss, H.-D. Meyer, L.S. Cederbaum, B. Engels, H.U. Suter, Temporary anions - calculation of energy and lifetime by absorbing potentials: The N_2^- $^2\Pi_g$ resonance. J. Phys. B **31**, 4107 (1998)
50. D. Zuev, T.-C. Jagau, K.B. Bravaya, E. Epifanovsky, Y. Shao, E. Sundstrom, M. Head-Gordan, A.I. Krylov, Caps within the eom-cc family of methods: Theory implementaion and benchmarks. J. Chem. Phys. **141**, 024102–1 (2014)
51. T. Sommerfeld, M. Ehara, Complex absorbing potentials with voronoi isosurfaces wrapping perfectly around molecules. J. Chem. Theory Comput. **11**, 4627 (2015)
52. Z. Benda, K. Rickmeyer, T.C. Jagau, Structure optimization of temporary anions. J. Chem. Theory Comput. **14**, 3468 (2018)